Physicochemical Study of Visible Light Photooxidation of Benzyl Ethers using Metal-Organic Frameworks

Undergraduate Research Report

Department of Chemistry

University of Central Florida

Fall 2014

Advisor: Dr. Fernando Uribe-Romo

Michelle Hettinger

Study of Visible Light Photooxidation of Benzyl Alcohols using Metal-Organic Frameworks

Michelle A. Hettinger
University of Central Florida

ABSTRACT: Metal-organic frameworks represent the merging of traditional molecular and solid-state catalysts. With their very large pore sizes and surface areas, tunable linkers and robust structures MOFs are leading candidates for future roles in many applications including photoredox catalysis. This work represents some of the first steps taken towards the development of MOFs as efficient visible light photoredox catalysts. It was found that MOFs containing Ti^{+4} and Zr^{+4} metal centers are photoredox active towards the oxidation of benzyl alcohols, observing photochemical quantum yields of about 4 percent.

Figure 1. Light generates a photoredox active state and the catalyst undergoes subsequent oxidation or reduction with organic molecules.

Introduction

Photoredox catalysis occurs when light is absorbed by a catalyst, and this catalyst achieves a light-induced charge separated state, which is redox active. This light activated redox catalyst, be able to either oxidize or reduce organic molecules (Figure 1). Photoredox catalysts can be classified as either homogeneous, where the catalyst is a molecular catalyst that exists in the same phase as the reactants or as heterogeneous, where the catalyst is an insoluble material suspended in solution, with the chemical reaction occurring at the interphase.

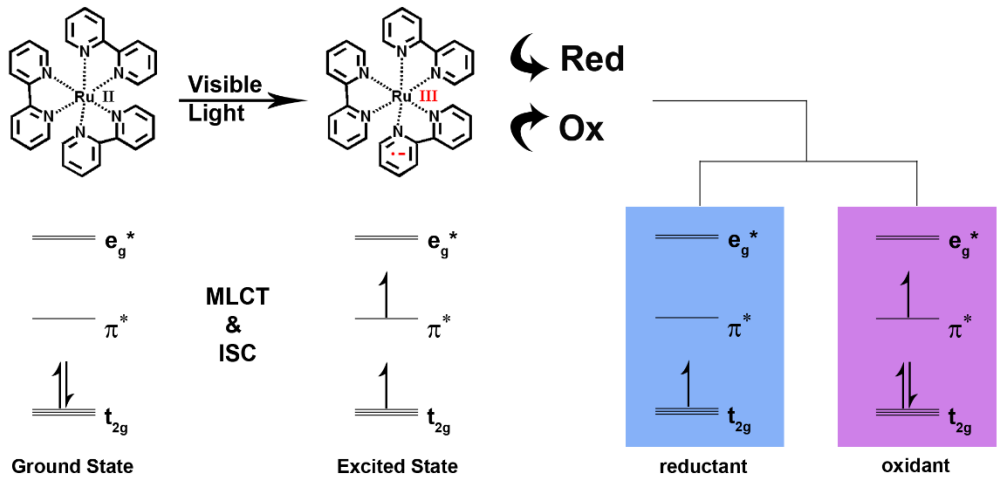

Figure 2. Tris(2,2'-bipyridine)ruthenium(II) undergoes a single electron metal to ligand charge transfer and subsequent intersystem crossing to give the lowest energy triplet excited state. The catalyst then acts as a reductant or an oxidant.

The Tris(2,2'-bipyridine)ruthenium(II) complex, $Ru(bpy)_3^{+2}$, serves as a good example for illustrating the properties of homogeneous catalysts (Figure 2). Upon absorption of visible light a metal to ligand charge transfer (MLCT) occurs and one electron from one of the t_{2g} orbitals of the metal is excited to a π^* orbital of the ligand[1]. This results in Ru(II) being oxidized to Ru(III) and the ligand reduced[1]. The singlet MLCT under goes rapid intersystem crossing (ISC) to give the lowest-energy triplet excited state, which has a long lifetime of 1100 ns[1]. In this excited triplet MLCT state the complex is able to act as a reductant when a molecule accepts the ligand-centered electron to give $Ru(bpy)_3^{+3}$, or it can act as an oxidant when a molecule donates an electron to the t_{2g} orbital to give $Ru(bpy)_3^{+}$. Furthermore, the bipyridine ligand may be modified to enhance selectivity towards specific reactions. For example reduction of hydrazides and hydrazines was accomplished with tris(bipyrazyl)ruthenium(II) and intramolecular [2+2] cycloaddition of styrenes with tris(bipyrimidine)ruthenium(II)[1].

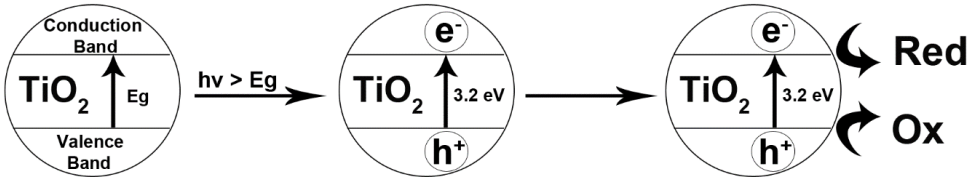

Figure 3. When TiO_2 is struck with light the charge separated state that is generated is the electron-hole pair, with the electron in the conduction band and the hole in the valence band.

On the other hand, hetergeneous photoredox catalysts, particularly titanium-oxides like rutile or anatase, are of interest due to their chemical stability, reusability, high reactivity and low toxicity[2]. As Figure 3 illustrates, when UV light strikes the catalyst an electron-hole pair is created with the electron in the conduction band and the hole in the valence band. In this state, the photoredox catalyst is able to act as a reductant by donating an electron to an organic molecule, or act as an oxidant by accepting an electron from an organic molecule. Although much research has been done into optimizing the band gap and lifetimes of the charge carriers, TiO_2 is mainly used in the evolution of hydrogen gas from water and decomposition of harmful organic materials because it does not possess the tunability for specific reactions that homogeneous catalysts[2].

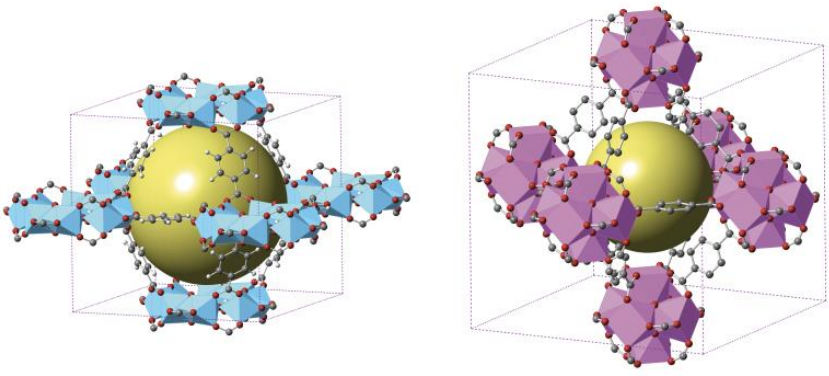

Figure 4. Unit cells of MIL-125 (left) and UiO-66 (right). The yellow sphere represents the volume of the pore size per unit cell.

Metal-organic frameworks (MOFs) are promising new materials with potential applications as improved photoredox catalysts as they merge properties of molecular and solid state materials. Figure 4 illustrates two MOFs (MIL-125 and UiO-66) generated in software with data obtained from previous works[3,4]. The structures of these MOFs have been included to help the reader gain a better visual conception of the properties shared amongst all MOFs. Metal-organic frameworks are comprised of transition metal-oxide clusters bound together by organic molecular linkers that form porous, crystalline materials with large surface areas[5]. Due to their crystallinity MOFs can be characterized by powder X-ray diffraction for a number of purposes. For example, an experimental PXRD pattern can facilitate in the identification of crystalline compounds, be used to determine the crystal structure of a new compound as well as to measure the extent of which a crystalline solid state powder has defects[6]. With the data taken from an experimental diffraction pattern, a MOFs crystal structure can be determined in computer software that produces a 3-Dimensional crystal structure, which can be examined within the software.

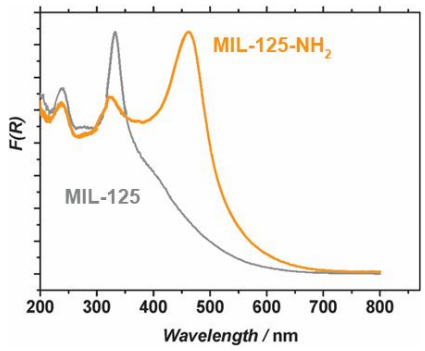

Figure 5. UV-Vis absorption spectra of MIL-125 (grey) and MIL-125-NH_2 (orange). Functionalizing with the NH_2 shifts the λmax from 350 to 500 nm, thus enhancing visible light absorption[7].

An interesting and desirable property of MOFs is their many possibilities for functionalization to enhance certain properties such as pore size and surface area[5], photochemical quantum yield and visible light absorption[7]. Figure 5 shows how functionalizing the MIL-125 MOF with an amino group on the terephthalate linker blue shifts the UV-vis absorption λmax out of the UV-region and into the visible spectrum[7].

Previous studies on the oxidation of benzyl alcohol into benzaldehyde showed that the MOF UiO-66-NH_2-X (*X* = -H, -F, -Cl, -Br) could catalyze this reaction. T.W. Goh et al. determined that the UiO-66-NH_2-F had the highest conversion (53.9%) and a turn over frequency (TOF) of 410 μmol min^{-1} $gram^{-1}$, whereas the UiO-66-NH_2 had TOF of 140 μmol min^{-1} $gram^{-1}$ and 18% conversion [8]. However this group did not report a photochemical quantum yield for any of the MOFs used to catalyze the oxidation of *p*-methoxybenzyl alcohol.

The aim of this research is to develop a model for investigating the photoredox capabilities of MOFs and their photochemical properties. The MOFs chosen for this research (vanadium based MIL-47-NH_2, titanium MIL-125-NH_2 and zirconium UiO-66-NH_2) all contain inexpensive transition metal centers with an amino terephthalic acid linker. Ideally the non-functionalized versions of these MOFs would also be studied, but due to time considerations only the MOFs with enhanced visible light absorption, due to the amino functional group were chosen to study. Kinetics for the visible light photooxidation of aromatic benzyl alcohols into benzaldehyde was measured by NMR spectroscopy to obtain a rate of reaction and photochemical quantum yields.

Additionally, steps were taken toward the synthesis of a new substrate for photocatalysis, the benzyl menthol ether, to experiment with catalyzing the de-protection of benzyl ethers.

Experimental

Section 1.1 Synthesis of Metal-Organic Frameworks

Synthesis of MIL-47-NH_2[9]

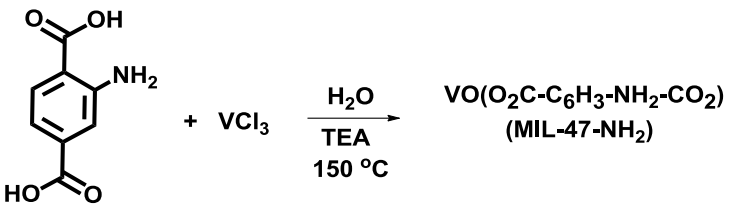

Scheme 1. Synthetic route for the preparation of MIL-47-NH_2.

Into a Teflon acid digestion bomb was added VCl_3 (0.142 g, 0.90 mmol) and 2-aminoterephthalic acid (0.041 g, 0.23 mmol) and diluted with 5.0 mL of deionized water and two drops of triethylamine. The acid digestion bomb was tightly capped and placed in an oven at 150 °C for 3 days. The obtained solid was filtered in a fine frit and washed with DMF (3 x 10 mL) and chloroform (3 x 10 mL). Yield: 32.0 mg (58% based on $VO_5C_8H_5N$).

Synthesis of MIL-125-NH_2[10]

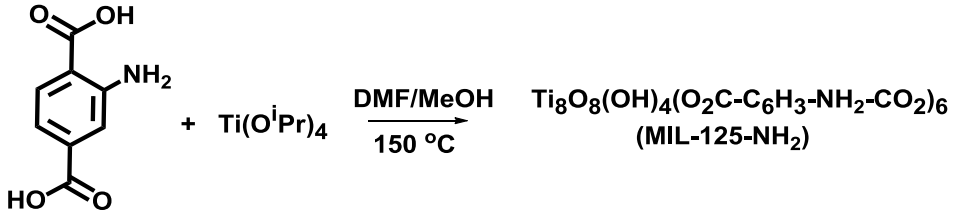

Scheme 2. Synthetic route for the preparation of MIL-125-NH_2.

Into a Teflon acid digestion bomb was added titanium isopropoxide (0.3 mL, 1.00 mmol) and 2-aminoterephthalic acid (0.4 g, 2.2 mmol) and diluted with 5.0 mL of a 9:1 –v:v mixture of DMF and Methanol. The acid digestion bomb was tightly capped and placed in an oven at 150 °C for 24 hours. The obtained solid was filtered in a fine frit and washed with chloroform (3 x 10 mL). Yield: 130 mg (66% based on $TiO(OH)_{1/2}(O_2C\text{-}C6H_3\text{-}NH_2\text{-}CO_2)_{3/4}$).

Synthesis of UiO-66-NH_2[11]

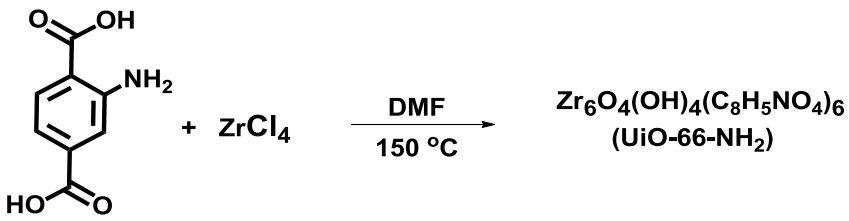

Scheme 3. Synthetic route for the preparation of UiO-66-NH_2.

Into a Teflon acid digestion bomb was added $ZrCl_4$ (0.05 g, 0.215 mmol) and 2-aminoterephthalic acid (0.078 g, 0.429 mmol) and diluted with 2.0 mL of DMF. The acid digestion bomb was sealed and placed in an oven at 150 °C for 24 hours. The obtained solid was filtered in a fine frit and washed with chloroform (3 x 10 mL). Yield: 82 mg (65% based on $ZrO_{2/3}(OH)_{2/3}(C_8H_5NO_5)$).

Section 1.2 Characterization of Metal-Organic Frameworks

Powder x-ray diffraction was performed on a Rigaku MiniFlex 600 with a Cu (Kα) X-ray source (λ = 1.414 Å) from the range of 0 to 50 degrees (2θ) with the voltage and current set to 40 kV and 15 mA respectively. The simulated diffraction patterns were obtained from published crystallographic data using Materials Studio 8.0.

Section 2.1 Photoreactor Setup

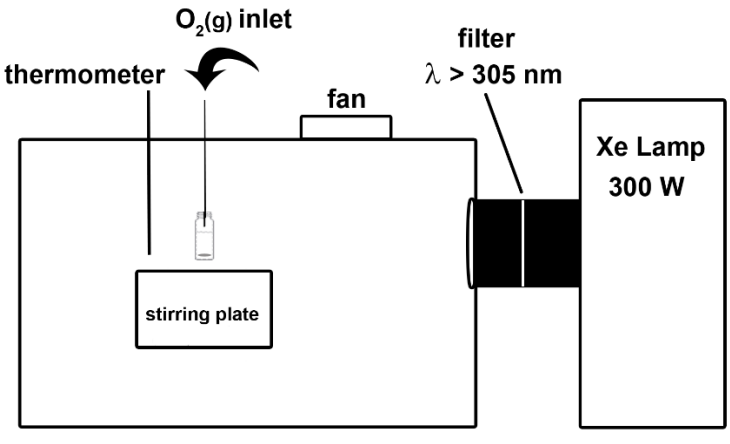

Figure 5. Photoreactor contains 300 W xenon lamp with 305 nm filter, thermometer and fan, and an inlet for oxygen gas.

All photochemistry experiments were performed using a Newport 69911 Xenon Arc Lamp set to a power of 300 W and with a Newport 20CGA-305 filter to filter out wavelengths below 305 nm. As Figure 5 illustrates, the photoreactor also has a fan and thermometer to maintain a temperature of 25 °C as well as a stir plate to ensure thorough mixing.

Section 2.2 Photocatalysis Sample Preparation

O_2*(g)* saturated acetonitrile was prepared by bubbling a constant flow of O_2*(g)* into anhydrous acetonitrile for 30 minutes. 4-methoxybenzyl alcohol was purified via Column Chromatography before use (SiO_2, 20% v/v EtOAc/Hexanes). 4-methoxybenzyl alcohol (0.168 g, 1.221 mmol) was loaded in a 20 mL glass scintillation vial and dissolved in 6.0 mL of anhydrous O_2*(g)* saturated acetonitrile. Mesitylene (85 μL, 0.608 mmol) was added via micropipette as an internal standard. The prepared solution was split into three portions into three 3 mL scintillation vials (Borosilicate Fisherbrand) containing a magnetic stirring bar. 8-10 mg of MOF was added (MOF = MIL-47-NH_2, UiO-66-NH_2, MIL-125-NH_2), and the vial was capped with a Teflon rubber cap. A rubber balloon with a needle attachment was willed with O_2*(g)* and the needle was inserted in the vial, with the tip of the needle in the middle of the head space, and the vial-balloon assembly was mounted in the photoreactor.

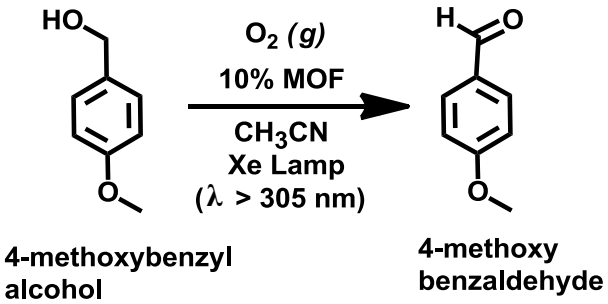

Scheme 4. Reaction scheme for the oxidation of 4-methoxybenzyl alcohol to4-methoxy benzaldehyde in the presence of MOF under oxygen atmosphere.

At each time (0, 2, 4, 6, 8, 12 and 24 h) a 20 μL sample was extracted via micropipette and diluted with 0.5 mL of $CDCl_3$ in a test tube. The dilute mixture was filtered through a 0.2 μm PTFE syringe membrane and transferred to a 5 mm NMR tube.

Section 3.1 Obtaining Rates of Reaction

Individual NMR spectra for a given experiment (0-24 hour samples) were stacked in processing software MNova and the absolute integration values were obtained for the following peaks: mesitylene Ar-H (6.78 ppm), 4-methoxybenzyl alcohol O-CH_3 (3.78 ppm) and 4-methoxybenzaldehyde O-CH_3 (3.88 ppm). The concentration of starting material at each time interval was calculated as the ratio of the integration of starting material to mesitylene multiplied by the actual concentration of mesitylene (101.5 mM). Similarly the concentrations of product were calculated as the ratio of the integration of product to that of mesitylene multiplied by the concentration of mesitylene. The equations are summarized below.

$$[\mathrm{SM}] \text{ or } [\mathrm{P}] = \frac{\text{Integration of } \mathrm{OCH_3}(\mathrm{SM} \text{ or } \mathrm{P})}{\text{Integration of } \mathrm{Ar-H}} \bullet 101.5 \text{ mM}$$

Plotted into a graph was concentration on the y-axis and time on the x-axis. The slope of this graph is the rate of the reaction in mM per minute.

Section 3.2 Quantum Yield[12]

$$\Phi_{\mathrm{rxn}} = \frac{\mathrm{R^{in}}_{\mathrm{rxn}}}{\mathrm{R^{in}}_{\mathrm{std}}} \Phi_{\mathrm{std}}$$

Heterogeneous photochemical quantum yields were calculated from the equation above, where the initial rate of reaction is the slope of the concentration vs. time plot, the initial rate of the standard is -239.0 +/- 19.2 μM/minute (as determined in our photochemical research by Dr. Yuen Lau) and the quantum yield of the standard is 0.22[12]. The standard reaction for which these values were obtained is the decomposition of *p*-cresol shown in the figure below.

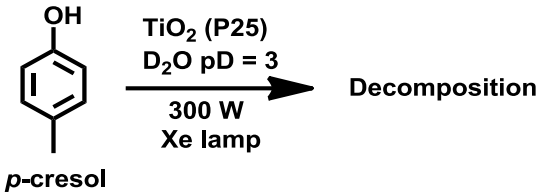

Scheme 5. Photocatalyzed decomposition of *p*-cresol with TiO_2 (P25) in D_2O at a pD of 3, $\Phi = 0.22$.

Section 4.1 Tosylation of 4-methoxybenzyl alcohol[13]

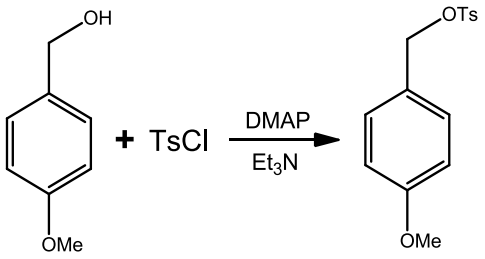

Scheme 6. Reaction scheme for tosylation of 4-methoxybenzyl alcohol.

Into a 50 mL round bottom flask was added 4-methoxybenzyl alcohol (0.5 g, 3.619 mmol), 4-Dimethylaminopyridine (0.111 g, 0.905 mmol) and trimethylamine (0.798 mL) and diluted with 18.0 mL of dichloromethane. In a separate, vial 4-toluenesulfonyl chloride (1.035 g, 5.428 mmol) was dissolved in 18.0 mL of DCM. The round bottom flask was brought to 0 °C and then the tosyl chloride solution was added dropwise into the reaction mixture. Observations by TLC showed the reaction was finished after 20 minutes. The crude product was extracted with 35.0 mL of water followed by saturated sodium bicarbonate (2 x 35 mL) and finally 10 mL of a brine solution. The organic layer was concentrated under vacuum. A mixture of products were obtained that could not be separated.

Section 4.2 Bromination of 4-methoxybenzyl alcohol[14]

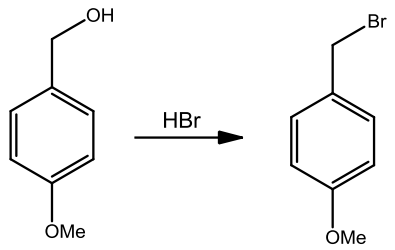

Scheme 7. Reaction scheme for bromination of 4-methoxybenzyl alcohol with HBr.

To a 10 mL round bottom flask was dissolved 4-methoxybenzyl alcohol into 3 mL of toluene. 5 mL 48% HBr(aq) solution were pipetted dropwise into the reaction mixture was. It was noted that an emulsion formed immediately with the first few drops of HBr, but disappeared upon complete addition of the HBr. After stirring for 22 hours at room temperature the reaction was determined to have reached completion by observing the disappearance of 4-methoxybenzyl alcohol by TLC. The crude reaction mixture was partitioned between diethyl ether and water, and extracted with diethyl ether (3 x 10 mL). The combined organic layers were dried with anhydrous sodium sulfate, filtered and concentrated under vacuum resulting in a dark brown oil. Yield: 531.7 mg (73%). ^{1}H NMR (400 MHz, $CDCl_3$, 25 °C) δ 7.33 (d, 2 H, *J* = 8.8 Hz) 6.87 (d, 2 H, *J* = 8.8 Hz) 4.51 (s, 2 H) δ 3.81 (s, 3 H).

Results and Discussion

Powder X-ray diffraction of the MOFs reveals the crystalline nature of the MOFs by the appearance of sharp Bragg peaks (Figure 6). Moreover, the simulated diffraction patterns for each MOF contained peaks at the same degrees (2θ) as their respective experimental pattern, suggesting that the MOFs had the expected crystal structure. The exception is the MIL-47-NH_2 MOF, which had at least one peak at 12 degrees (2θ) in the simulated pattern that is not in the experimental. This was because the MOF structure can “breathe”, or expand and contract with the input or output of gas, and these changes in the structure result in changes in the d-spacing and thus the position

of the Bragg peaks are shifted[9,15]. These diffractograms confirm the successful preparation of the MOFs.

Powder X-ray Diffraction of MOFs

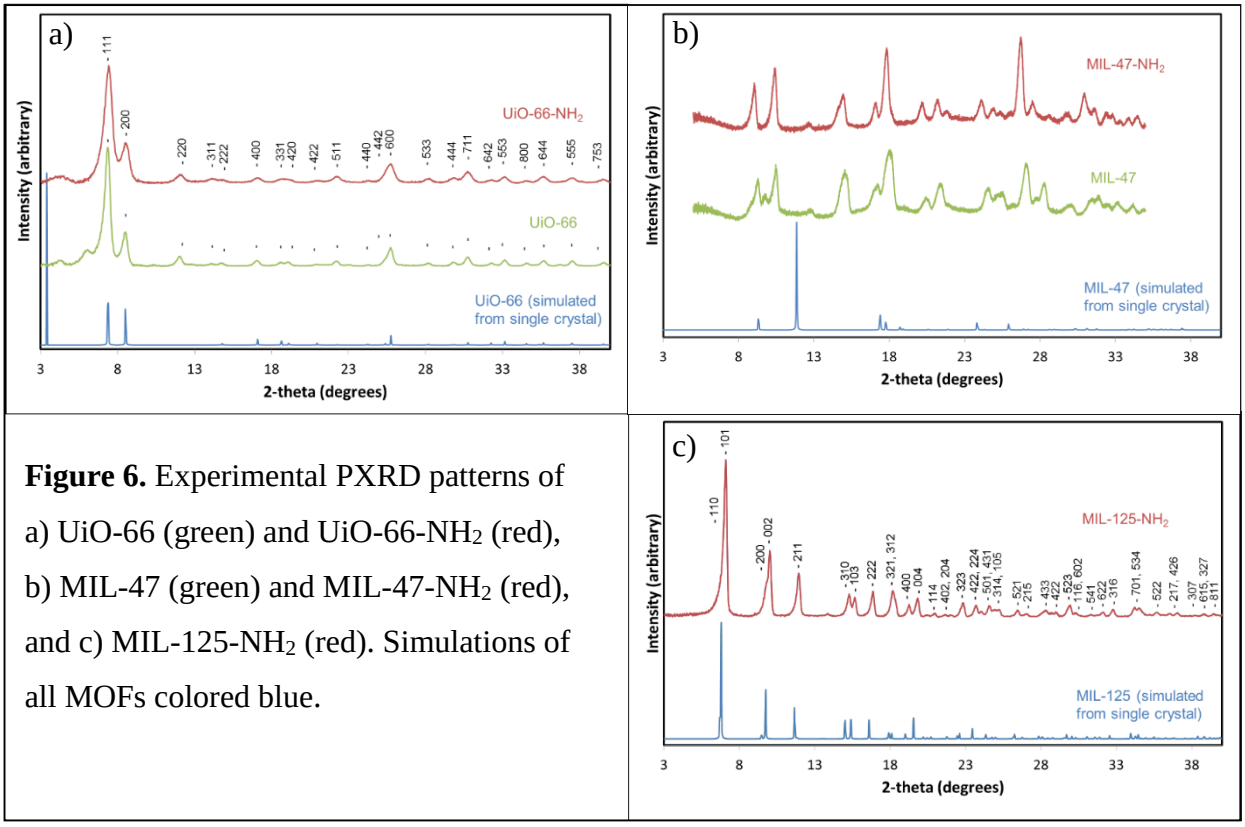

Figure 6. Experimental PXRD patterns of a) UiO-66 (green) and UiO-66-NH_2 (red), b) MIL-47 (green) and MIL-47-NH_2 (red), and c) MIL-125-NH_2 (red). Simulations of all MOFs colored blue.

Monitoring Kinetics by ^{1}H NMR Spectroscopy

^{1}H NMR of the aliquots taken over the course of each kinetics run, and are stacked in Figure 7 to illustrate the formation of product over time. There lies a singlet at 3.79 ppm from the methoxy peak of the benzyl alcohol and when converted into benzaldehyde over 24 hours that peak shifted to 3.88 ppm. Aromatic protons from mesitylene had a chemical shift of 6.78 ppm and since mesitylene was held at a constant concentration this peak was used as a reference for which the actual concentrations of reactants and products were calculated.

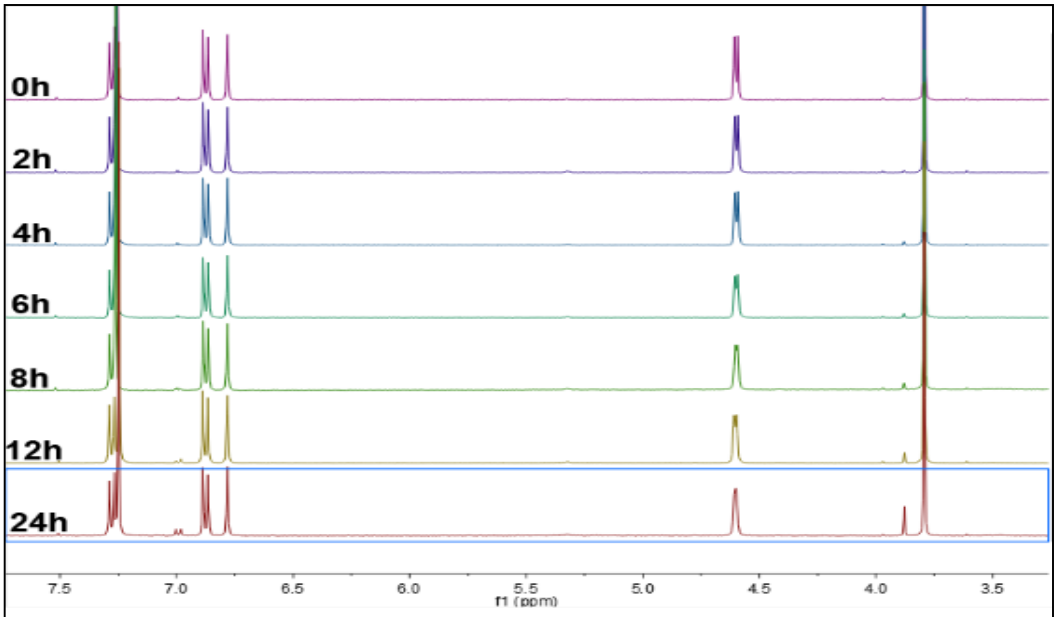

Figure 7. Stacked ^{1}H NMR shows oxidation of 4-methoxybenzyl alcohol over the course of a 24 hour period.

Rates of Reaction and Quantum Yield

Plotting the concentrations of starting material to product vs time reveal a linear dependence with time, suggesting a zero order reaction kinetics (Figures 8). Zero order rate laws are typical of heterogeneous reactions. The catalytic performance of MIL-125-NH_2 and UiO-66-NH_2 were of similar slopes of -40.5 and -43.7 μM/minute respectively, and total conversions of 13 and 12 percent respectively. MIL-47-NH_2, however, was observed to have no catalytic activity as the percent conversion of alcohol to aldehyde was only 1% (rate = -5.0 μM/minute), which was close to the conversion obtained in the absence of MOF.

Heterogeneous photochemical quantum yields were calculated (Table 1) to be 3.7 and 4.0% for MIL-125-NH_2 and UiO-66-NH_2 respectively, while MIL-47-NH_2 had a quantum yield of 0%. A quantum yield of 4% means that four percent of the photons striking the MOFs oxidize a benzyl alcohol molecule.

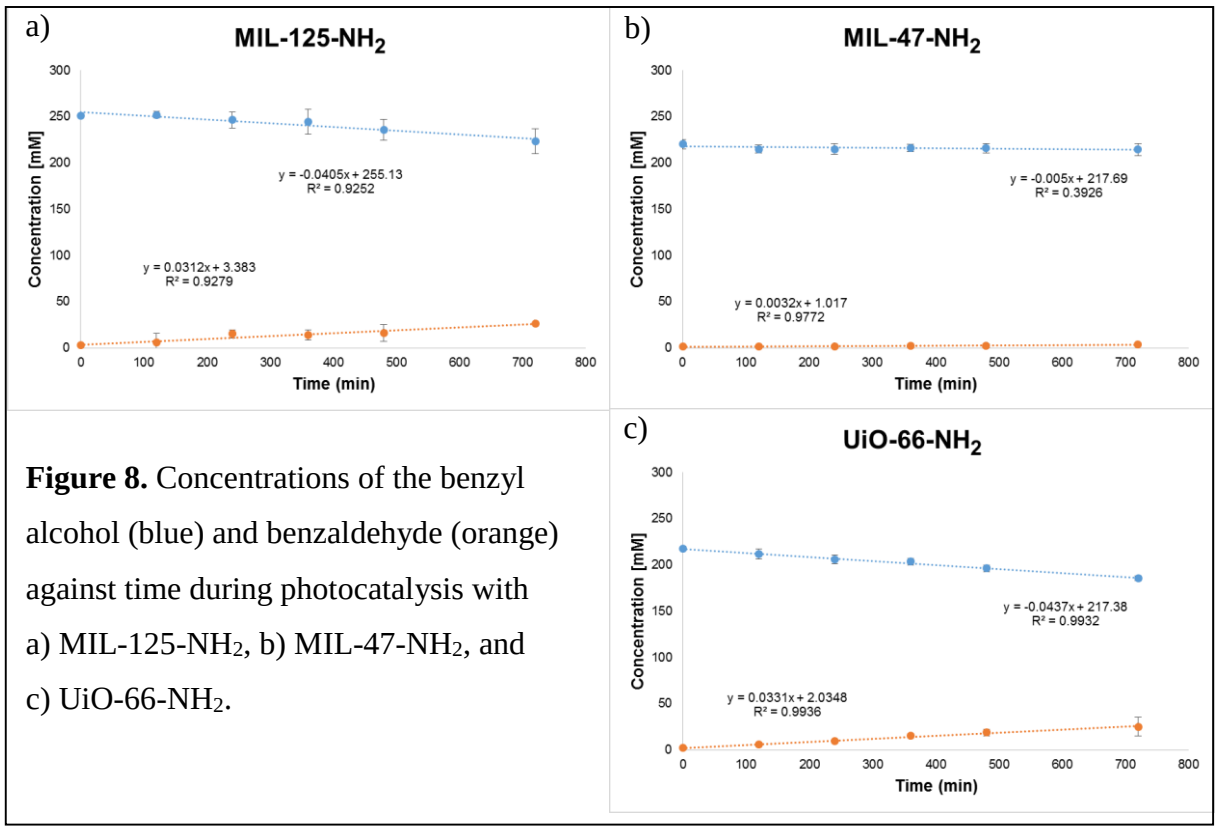

Figure 8. Concentrations of the benzyl alcohol (blue) and benzaldehyde (orange) against time during photocatalysis with a) MIL-125-NH_2, b) MIL-47-NH_2, and c) UiO-66-NH_2.

Table 1. Rates of reactions and photochemical quantum yields.

MOF	Rate (µM/min)	Quantum Yield
Standard	**-239.0 +/- 19.2**	**0.22 +/- 0.04**
MIL-125-NH_2	**-40.5 +/- 9.0**	**0.037 +/- 0.011**
MIL-47-NH_2	**-5.0 +/- 4.8**	**0.0046 +/- 0.0045**
UiO-66-NH_2	**-43.7 +/- 3.5**	**0.040 +/-0.009**

Tosylation of 4-methoxybenzyl alcohol

The ^{1}H NMR spectrum for the product of this reaction (Figure 9) reveals that even though the starting material was absent on TLC the tosylated product was only a minor product dominated by the presence of 4-methoxybenzyl chloride since OTs is a better leaving group[16].

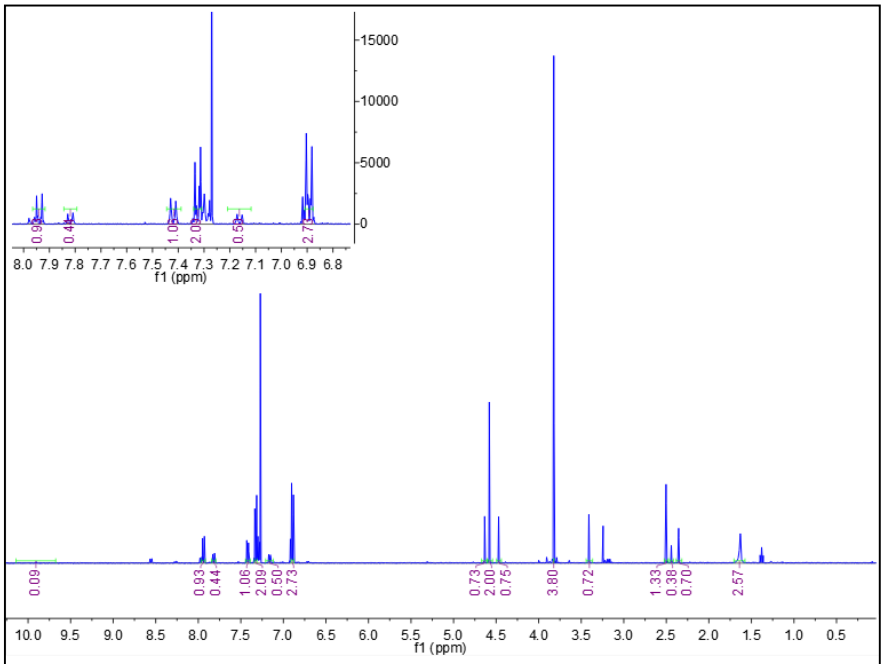

Figure 9. ^{1}H NMR of tosylation shows mixture of products, mainly 4-methoxybenzyl chloride.

Bromination of 4-methoxybenzyl alcohol

The ^{1}H NMR spectrum for the product of this reaction (Figure 10) confirmed the presence of 4-methoxybenzyl bromide. The methoxy methyl appeared as a singlet at 3.81 ppm with an integration of 3, benzyl CH_2 at 4.51 ppm with an integration of 2 and the two sets of doublets at 6.87 and 7.33 ppm with integrations of 2 were from the aromatic protons. This product will be used in the preparation of benzyl ethers.

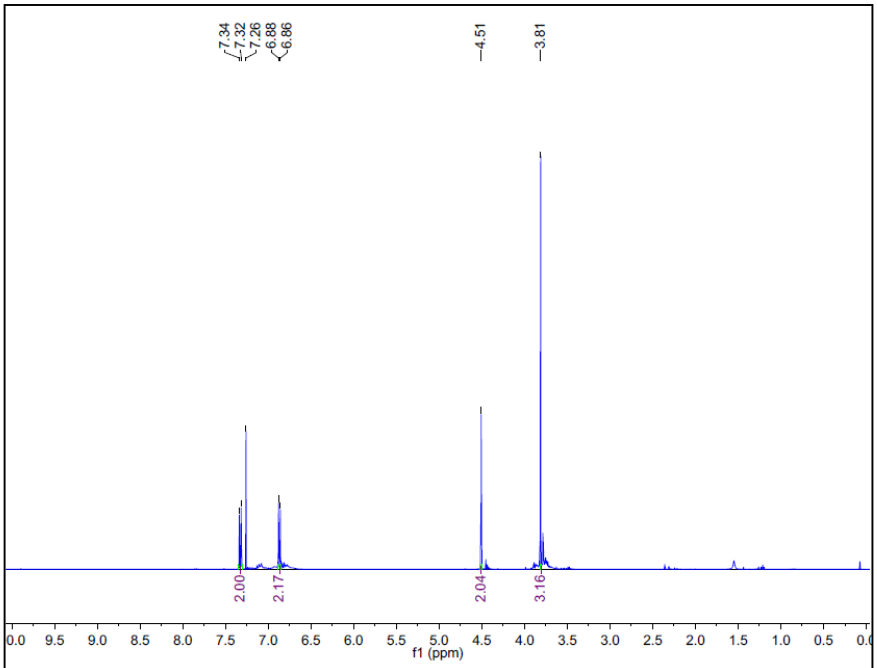

Figure 10. ^{1}H NMR of 4-methoxybenzyl bromide.

Conclusions

This work demonstrates that MOFs can be used as visible light photoredox catalysts, particularly in the oxidation of benzyl alcohols. However, the MOFs were not necessarily as efficient as expected. For one the quantum yields were over five times less for the MOFs (Φ = 0.04) than the TiO_2 standard they were compared to (Φ = 0.22). Additionally it was concluded that the reaction is taking place at the surface of the MOF and that the full extent of the MOFs surface area within the pores is not being utilized. Future work on the temperature dependence of the photooxidation of benzyl alcohols could demonstrate whether or not the reaction is limited by the ability of reactant molecules to diffuse into and out of the MOF.

Steps taken toward the synthesis of menthol ester were thwarted by unstable intermediate products such as the unstable 4-methoxybenzyl bromide, or formation of major side products as was the case in the attempt to tosylate the benzyl alcohol. However a new scheme was proposed

(Figure 11) to obtain the menthol ester (**3**) to be used in the visible light photocatalysis of the deprotection of benzylic ethers.

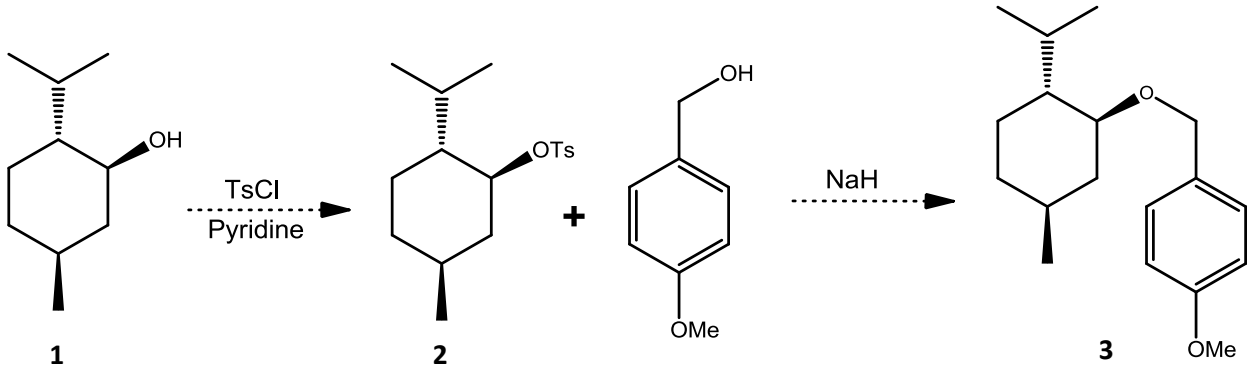

Figure 11. Proposed reaction scheme for menthol ester involves tosylation of menthol (**1**) in pyridine to get **2**, followed by NaH and 4-methoxybenzyl alcohol to get **3**.

References

1. Prier, C. K.; Rankic, D. A.; MacMillan, D. W. C., Visible Light Photoredox Catalysis with Transition Metal Complexes: Applications in Organic Synthesis. *Chem. Rev.* **2013,** *113*, 5322-5363.
2. Schneider, J.; Matsuoka, M.; Takeuchi, M.; Zhang, J.; Horiuchi, Y.; Anpo, M.; Bahnemann, D. W., Understanding TiO2 Photocatalysis: Mechanism and Materials. *Chem. Rev.* **2014,** *114*, 9919-9986.
3. Dan-Hardi, M., Serre, C., Frot, T., Rozes, L., Maurin, G., Sanchez, C., and Ferey, G., A new Photoactive Crystallline Highly Porous Titanium (IV) Dicarboxylate. *Journal of the American Chemical Society*, **2009**, Volume *131*, 10857-10859.
4. Cavka, J. H., Jakobsen, S., Olsbye, U., Guillou, N., Lambertie, C., Bordiga, S., and Lillerud, K. P., A New Zirconium Inorganic Building Brick Forming Metal Organic Frameworks with Exceptional Stability. *Journal of the American Chemical Society*, **2008**, Volume *130*, 13850-13851.
5. Chen, T.-H.; Popov, I.; Kaveevivitchai, W.; Miljanic, O. S., Metal-Organic Frameworks: Rise of the Ligands. *Chem. Mater.* **2014,** *26*, 4322-4325.
6. West, A. R., *Solid State Chemistry and its Applications*. Second ed.; 2014.
7. Nasalevich, M. A.; Goesten, M. G.; Savenije, T. J.; Kapteijna, F.; Gascon*a, J., Enhancing optical absorption of metal–organic frameworks for improved visible light photocatalysis. *Chemical Communications* **2013,** *49*, 10575-10577.

8. Goh, T. W.; Xiao, C.; Maligal-Ganesh, R. V.; Li, X.; Huang, W., Utilizing mixed-linkerzirconiumbasedmetal-organicframeworks to enhance the visible light photocatalytic oxidation of alcohol. *Chemical Engineering Science* **2015,** *124*, 45-51.
9. Barthelet, K.; Marrot, J.; Riou, D.; Ferey, G., A Breathing Hybrid Organic-Inorganic Solid with Very Large Pores and High Magnetic Characteristics. *Angew. Chem. Int. Ed.* **2002,** *41*, 281-284.
10. Im, J. H.; Kang, E.; Yang, S. J.; Park, H. J.; Kim, J.; Park, C. R., Simple Preparation of Anatase Titanium Dioxide Nanoparticles by Heating Titanium-Organic Frameworks. *Bulletin of the Korean Chemical Society* **2014,** *35*, 2477-2480.
11. Schaate, A.; Roy, P.; Godt, A.; Lippke, J.; Waltz, F.; Wiebcke, M.; Behrens, P., Modulated Synthesis of Zr-Based Metal–Organic Frameworks: From Nano to Single Crystals. *Chemistry - A European Journal* **2011,** *17*, 6643-6651.
12. Serpone, N.; Salinaro, A., Terminology, relative photonic efficiencies and quantum yields in heterogeneous photocatalysis. Part I: Suggested protocal. *Pure Appl. Chem.* **1999,** *71*, 303-320.
13. Katakawa, K.; Yonenaga, D.; Terada, T.; Aida, N.; Sakamoto, A.; Hoshino, K.; Kumamoto, T., Selective Synthesis of Benzyl Enol Ethers of β-Dicarbonyl Compounds in Basic Condition and the Application towards Synthesis of Naphthoquinones. *Heterocycles* **2014,** *88*, 817-825.
14. Bull, S. D.; Davies, S. G.; Epstein, S. W.; Garner, A. C.; Mujtaba, N.; Roberts, P. M.; Savory, E. D.; Andrew D. Smith, a.; Tamayoa, J. A.; Watkinb, D. J., Enantiodiscrimination of racemic electrophiles by diketopiperazine enolates: asymmetric synthesis of methyl 2-amino-3-aryl-butanoates and 3-methyl-aspartates. *Tetrahedron* **2006,** *62*, 7911-7925.
15. Biswas, S.; Ahnfeldt, T.; Stock, N., New Functionalized Flexible Al-MIL-53-X (X = -Cl, -Br, -CH3, -NO2, -(OH)2) Solids: Syntheses, Characterization, Sorption, and Breathing Behavior. *Inorganic Chemistry* **2011,** *50*, 9518-9526.
16. Ding, R.; He, Y.; Wang, X.; Xu, J.; Chen, Y.; Feng, M.; Qi, C., Treatment of Alcohols with Tosyl Chloride Does Not always Lead to the Formation of Tosylates. *Molecules* **2011,** *16*, 5665-5673.